Optimal design and operation of electrodialysis for brackish-water desalination and for high-salinity brine concentration

Citation: Chehayeb, Karim M. et al. "Optimal Design and Operation of Electrodialysis for Brackish-Water Desalination and for High-Salinity Brine Concentration." Desalination 420 (October 2017): 167–182 © 2017 Elsevier

As Published: http://dx.doi.org/10.1016/J.DESAL.2017.07.003

Publisher: Elsevier

Persistent URL: http://hdl.handle.net/1721.1/113009

Version: Author's final manuscript: final author's manuscript post peer review, without publisher's formatting or copy editing

Optimal design and operation of electrodialysis for brackish-water desalination and for high-salinity brine concentration

Karim M. Chehayeb[a,*], Daniel M. Farhat[b,*], Kishor G. Nayar[a], John H. Lienhard V[a,**]

[a] *Department of Mechanical Engineering, Massachusetts Institute of Technology, Cambridge, MA 02139, USA.*
[b] *Department of Mechanical Engineering, American University of Beirut, Beirut, Lebanon.*

Abstract

Electrodialysis (ED) is a desalination technology that has been deployed commercially for decades. However, few studies in the literature have looked at the optimal design and operation of these systems, especially for the concentration of high-salinity brines. In this paper, a set of constraints is defined to allow a fair comparison between different system sizes, designs, and operating conditions. The design and operation of ED are studied for the applications of brackish-water desalination and of high-salinity brine concentration for a fixed system size. The set of variables that determine the power consumption of a fixed-size system is reduced to include only the channel height and the velocity, with all the other design and operation variables depending on these two variables. After studying the minimization of power consumption for a fixed system size, the minimum costs associated with the different system sizes are studied, and the differing trends in brackish-water and high-salinity applications are compared. Finally this paper presents the effect of the cost modeling parameters on the trends of the optimal system size, current density, length, channel height, and velocity for the two applications studied.

Keywords: electrodialysis, optimization, brackish, high salinity, brine concentration

Citation: K.M. Chehayeb, D.M. Farhat, K.G. Nayar, J.H. Lienhard V, "Optimal design and operation of electrodialysis for brackish-water desalination and for high-salinity brine concentration," Desalination, **420**:167-182, 15 Oct. 2017.

*Co-first author
**Corresponding author
Email address: lienhard@mit.edu (John H. Lienhard V)

Nomenclature

Acronyms

AEM	Anion-exchange membrane
CEM	Cation-exchange membrane
MS	Maxwell-Stefan

Symbols

A	effective cell-pair area [m^2]
a	activity [-]
C	cost [\$/m^3 product]
c^*	normalized cost [(\$/m^3 product)/(\$/kWh)]
c	concentration [mol/m^3]
D	diffusion coefficient of salt [m^2/s]
$Đ_{ij}$	Maxwell-Stefan diffusion coefficient for species i and j [m^2/s]
F	Faraday constant, 96,487 [C/mol]
f	friction factor [-]
h	channel height [m]
i	current density [A/m^2]
i	annual interest rate [-]
J	flux [mol/m^2-s]
K_e	cost of electricity [\$/W-s]
K_m	fixed cost per unit cell-pair area per unit time [\$/m^2-s]
$K_\mathrm{m}, 0$	fixed cost per unit cell-pair area per unit time at time 0 [\$/m^2-s]
k_m	mass transfer coefficient [m/s]
L	effective stack length [m]
L_s	salt permeability [m/s]
L_w	water permeability [mol/m^2-s-bar]
m	molality [mol/kg]
N	molar flow rate [mol/s]
N_cp	number of cell pairs [-]
P	power consumption [W]
Q	volumetric flow rate [m^3/s]
R	universal gas constant, 8.3145 [J/mol-K]
Re	Reynolds number, Eq. F.5 [-]
r	electric resistance [Ω-m^2]
r	cost ratio, Eq. 9 [W/m^2]
S	salinity [g/kg]
Sc	Schmidt number, Eq. F.6 [-]
Sh	Sherwood number, Eq. F.1 [-]
T	absolute temperature [K]
T_s	salt transport number [-]
T_w	water transport number [-]
V	voltage [V]

v	velocity (at the product outlet) [m/s]
W	stack width [m]
z	charge number

Greek

Δ	difference or change
∇	gradient
ε	spacer volume fraction [-]
Φ	electric potential [V]
$\gamma_{\pm}$	mean molal (or molar) activity coefficient [-]
μ	dynamic viscosity [Pa-s]
μ_i	electrochemical potential of ion i [J/mol]
μ_{s}	chemical potential of the salt [J/mol]
μ_{w}	chemical potential of water [J/mol]
π	osmotic pressure [bar]
τ	plant life [years]
ρ	density [kg/m^3]

Subscripts

avg	average
C	concentrate
cp	cell-pair
D	diluate
i	ion i
m	at membrane interface
s	salt
w	water

Superscripts

m	in membrane
s	in solution

1. Introduction

Electrodialysis (ED) is a desalination technology that uses an electric work input and ion-exchange membranes to move salt from a diluted solution to a concentrated solution. ED has successfully been used for the desalination of brackish water [1–9], and for the concentration of seawater [10, 11] or reverse-osmosis brine for salt production [1, 12, 13]. Despite the large number of studies published on ED, only a small number of these has analyzed the optimal design and operation of ED systems, with the bulk of the work being focused on brackish-water desalination. Select studies on the optimal design and operation of ED systems are described below.

Sonin and Isaacson [14] presented a dimensional analysis of a general electrochemical system where fluid flow enhanced the limiting current density. They presented two conditions for optimal hydrodynamic design, which they defined as the choice of the channel geometry and the flow speed in the channels. The first condition required operating at a low-enough current density such that the negative effects of concentration polarization are negligible. The second condition required a velocity low enough for the pumping cost to be much smaller than the capital costs of the system. They also stated that the channel height should always be minimized. They applied this dimensional analysis to the example of brackish-water ED to determine the optimal spacer design and to identify areas for improvement.

Hattenbach et al. [15] studied the effects of the flow velocity and the channel height on the cost of electrodialysis. They reported that velocity affected the pumping power and the limiting current density while the channel height affected both the pumping power and the ED stack power. The current was always set to 70% of the limiting current density, so that the velocity set the operating current and the required membrane area. They concluded that the channel height should be minimized, and they specified a range of velocities that minimized the total cost.

Nikonenko et al. [16] minimized the system cost by varying the channel height and the stack voltage, but they fixed the length of the system and did not vary the velocity as an independent variable. They concluded that the channel height should be small and that the velocity should be large so that the required area and the ED power consumption are decreased.

Lee et al. [2] set the applied current density to a fixed fraction of the limiting current density. They concluded that the cost of desalination of brackish water using ED is minimized at the highest possible limiting current density. However, as will be shown later in this paper, this conclusion was reached only because Lee et al. did not include the pumping power in their cost calculation.

Tsiakis et al. [7] accounted for pumping power in their optimization, but they also set the operating current at a fixed fraction of the limiting current density.

Turek [17] studied the effect of channel height on the performance of a fixed-size electrodialysis stack. The current density was set to a fixed fraction of the limiting current density, and an intermediate channel height was found to be optimal.

Choi et al. [18] determined the optimal current density based on capital costs, maintenance costs, ED stack power, and pumping power. However, they studied a batch system that operated at a fixed circulating velocity.

While the studies described above have studied the effect of select parameters on the design of ED systems, none of them comprehensively included the effects of all the important variables on the optimal design of ED systems. Thus, important trade-offs between variables were missed. For example, in several studies, the ratio of the applied current density to the limiting current density was kept constant, leading to the trade-off between ED power consumption and pumping power being poorly captured. Additionally, in some studies, the length of the system or the flow velocity was held constant, limiting the optimization possible. This has led to an incomplete understanding of how ED systems should be designed and operated. In this paper, a set of constraints is defined to allow a fair comparison of the different designs and operating points. To fully optimize ED systems, and to reach general conclusions, it is essential that no design variables be held constant. The approach presented is applied to brackish-water desalination and to high-salinity brine concentration. The constraints needed for a fair comparison between different designs and operating points are discussed in detail in Section 2 while the analytical ED models used in our analysis are discussed in Section 3.

2. Constraints for a fair comparison between different designs and operating points

In order to determine the optimal design and operation of an ED system, it is essential to decide on a set of system constraints that results in a fair comparison between the different designs and operating points. In deciding on these constraints, we can think about a general desalination or water treatment system which takes in a fixed amount of feed at a fixed salinity and is required to treat this feed to result in a fixed flow rate of product at a set salinity. Allowing different systems to treat different amounts of feeds with different recoveries or different product quality would result in an unfair comparison between these systems. In this study, we consider two different applications of ED: a) brackish-water desalination which takes a feed at 3 g/kg, and desalinates it to a product at 0.35 g/kg with a recovery of 80%, where recovery is defined as the ratio of the mass flow rate of the product to that of the feed; and b) high-salinity brine concentration which takes in seawater-desalination brine at 70 g/kg (e.g., the discharge from reverse osmosis or multi-stage flash) and concentrates it to 200 g/kg such that the diluted stream leaves at 35 g/kg, which represents the salinity

of seawater. We note that setting the inlet and outlet stream salinities also sets the recovery, which in this case is around 21%.

Figure 1 shows the configurations used and the specified inlet and outlet salinities. In the brackish-water application, the brine is recirculated to ensure high recovery. In addition, the channel height and the flow rate in the concentrate and diluate channels are the same. These two constraints determine the amount of brine that is recirculated. A species balance is performed where mixing occurs to calculate the concentrate salinity at the stack inlet. In the brine-concentration application, the channel height is the same in the two channels, but the flow rates need to be different to result in the set recovery ratio. The diluate stream is not recirculated because this would result in a significant drop in its concentration and in an increase in the stack resistance. Additional details on the configurations used are presented in Appendix C.

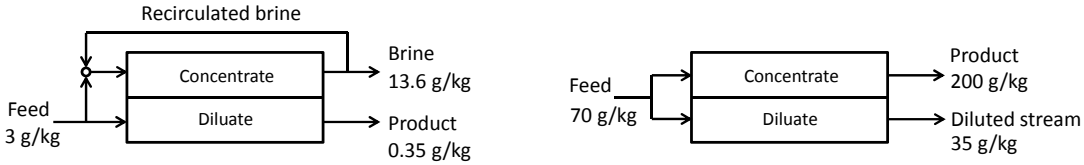

(a) Brackish-water desalination.

(b) High-salinity brine concentration.

Fig. 1: Configurations and salinities used in the two cases studied.

After setting the general constraints for a fair comparison, we look at the variables that influence the cost and performance of the system. To better understand the effect of the design and operation of the system on its energetic performance, we first study the different designs and operating points at a fixed system size, i.e., a fixed total membrane area. We assume that the fixed costs of the system are directly proportional to the membrane area, which means that fixing the membrane area sets the fixed costs of the system. This condition means that, when comparing different systems with the same area, it is only important to study their power consumption.

The performance and cost of an ED system are fully determined by the following variables: the feed and product salinities, S_{feed} and S_{product}, the feed and product flow rates, Q_{feed} and Q_{product}, the cell-pair area, A, the length of the stack, L, the width of the stack, W, the number of cell pairs, N_{cp}, the product flow velocity at the outlet, v, the channel height (the distance between two membranes), h, and the applied voltage, V, with some of these variables being dependent on others in the set. These variables are shown in Fig. 2. We note that membrane properties affect the system performance and cost, and should ideally be considered in the optimization of system performance. This can be done by repeating this analysis for different membranes, and by taking the different membrane costs into consideration when comparing the different systems. In this paper, however, we use only one set of ion-exchange membranes for each application, and we focus on the

analysis of the design and operation variables listed above.

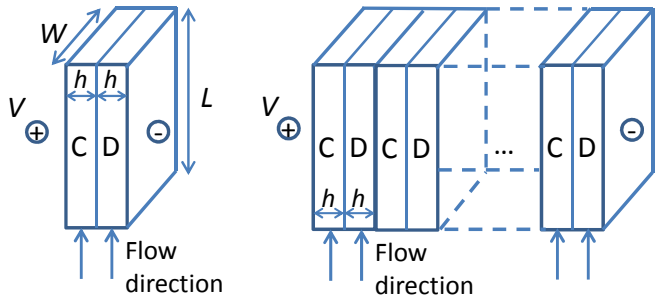

(a) Dimensions of a cell pair.

(b) A stack of N_{cp} cell pairs.

Fig. 2: Schematic diagrams of a cell pair and a stack of N_{cp} cell pairs. V is the applied voltage, L is the stack length, W is the stack width, and h is the channel height.

We start by reiterating that the inlet and outlet flow rates and salinities are set by the application and will be the same for all the systems studied in each of the two applications. In addition, we first study the operation of systems with the same area. This leaves us with the following set of variables: $\{L, W, N_{cp}, v, h, V\}$. Further, we note that when the following variables are set, $\{L, W, N_{cp}, v, h\}$, only one voltage results in the required product salinity, which means that the voltage can be considered as a dependent variable and does need to be considered as an operating variable.

The stack power consumption can be expressed as:

$$P_{stack} = V_{tot} i_{avg} A_{cp} \tag{1}$$

where V_{tot} is the total applied voltage, i_{avg} is the area-averaged current density, and A_{cp} is the cell-pair area. For a system with one cell pair, $V_{tot} = V_{cp}$, $A_{cp} = LW_{tot}$, and the stack power consumption is

$$P_{stack} = V_{tot} i_{avg} A_{cp} = V_{cp} i_{avg} L W_{tot} \tag{2}$$

We note that a system with a single cell pair is not feasible because the electrode potential drop would be very significant. However, this example is only used to show how the number of cell pairs and the stack width can be combined into one variable. For a system with N_{cp} cell pairs, $V_{tot} = N_{cp} V_{cp}$, $A_{cp} = LW_{cp}$, and the power consumption is

$$P_{stack} = V_{tot} i_{avg} A_{cp} = N_{cp} V_{cp} i_{avg} L W_{cp} \tag{3}$$

Equations 2 and 3 show that, as long as $W_{tot} = W N_{cp}$, and as long as the electrode voltage drop can be neglected, the number of cell pairs does not change the power consumption. The number of cell pairs, N_{cp},

contributes to the power consumption either through the voltage or through the cell-pair area. If the electric circuits of the two cases are analyzed, it can be shown that the system with N_{cp} cell pairs places the cell pairs in series, whereas the system with one cell pair effectively places N_{cp} cell pairs in parallel, such that the current density in the two cases is the same.

Combining W and N_{cp} into one variable results in the system performance depending only on the following variables: $\{L, N_{\mathrm{cp}}W, v, h\}$. These four variables are interdependent, such that only two of them can be independent. We can write the following expression for the product flow rate:

$$Q_{\mathrm{product}} = vh\,(N_{\mathrm{cp}}W) \tag{4}$$

and the following expression for the total cell-pair area:

$$A = L\,(N_{\mathrm{cp}}W) \tag{5}$$

We initially considered setting the length and width of the system as the independent variables, but results showed that the best independent variables to vary were the channel height and the flow velocity because they have the strongest direct effects on the power consumption. The stack power consumption strongly depends on the channel height, and the pumping power depends strongly on the velocity and on the channel height.

In summary, for a system of fixed area, we study the effects of the velocity and the channel height on the total power consumption. Setting these two independent variables fully determines the system design and operation as discussed in detail in this section. After studying the design and operation of a system of fixed area, we move towards modeling the costs of the different system sizes (each operated at the optimal channel height and velocity) to be able to find the optimal system size. In addition, all of the results in this work are normalized to systems resulting in 1 m^3/s of product. This normalization allows calculation of the system size, power consumption, and cost required for any capacity of production, with the design and operation variables such as the channel height, the velocity, and the length left unchanged for different production capacities.

3. Modeling

The modeling required to calculate the costs associated with an ED system consists of two parts. The first is the prediction of the performance of the electrodialysis system under different designs and operating conditions, and the second is the determination of the cost of these systems.

3.1. Modeling electrodialysis

The main goal of the electrodialysis model is to calculate the current density and the salt and water fluxes that result from an applied voltage. The voltage can be related to the current density by dividing the electric circuit into several resistances and electric potential drops in series:

$$V_{\mathrm{cp}} = \left(r_{\mathrm{bulk,C}} + r_{\mathrm{bulk,D}}\right) i + \Delta\Phi_{\mathrm{CEM}} + \Delta\Phi_{\mathrm{AEM}} + \Sigma_{j=1}^{4}\Delta\Phi_{\mathrm{film,j}} \tag{6}$$

where i is the current density. $r_{\mathrm{bulk,C}}$ and $r_{\mathrm{bulk,D}}$ are the bulk resistances in the concentrate and diluate channels, respectively. The bulk resistances are calculated from experimental data on conductivity [19–21]. $\Delta\Phi_{\mathrm{CEM}}$ and $\Delta\Phi_{\mathrm{AEM}}$ are the electric potential drops across the membranes, including the associated Donnan potentials at each interface, and $\Delta\Phi_{\mathrm{film,j}}$ is the electric potential drop in each of the four diffusion films between the membrane and the bulk.

To include the effect of the velocity on the performance of electrodialysis, the stagnant film model is used, and the thickness of the diffusion film, δ, is calculated from the Sherwood number correlation developed by Kuroda et al. [22], as presented in Appendix F. The concentration and electric potential profiles inside the diffusion films are calculated using the Maxwell-Stefan model as described in Appendix A. These profiles include the concentration in the solution at each membrane interface.

The membranes characterized by Kraaijeveld et al. [23] are only appropriate for brackish-water applications, and, as a result, the Maxwell-Stefan-based model is only used to predict the transport of salt and water through the membranes in the brackish-water desalination case. The details of this model have been laid out in previous studies [23, 24], and the major points of the model are summarized in Appendix B.1. In modeling high-salinity brine concentration, the model developed by Fidaleo and Moresi [25] is used with coefficients measured by McGovern et al. [26] at high salinity. The major points of this model are summarized in Appendix B.2. One of the outputs of these models is the current density, which is used in the calculation of the stack power consumption.

The calculated salt and water fluxes are used to modify the quantities of salt and water flowing through each channel. The electrodialysis stack is discretized and the finite-difference method is used to maintain a species balance, as described in Appendix C.

In addition to predicting the performance of an electrodialysis stack, we need to calculate the pumping power required to ensure the flow of the solutions through the stack. A pumping efficiency of 70% is assumed, and the friction factor correlation developed by Kuroda et al. [22] is used to ensure coherence between the effects of the spacer on mass-transfer enhancement and friction losses. The details of these calculations are presented in Appendix F.

3.2. Cost modeling

To calculate the cost of an electrodialysis system, the fixed costs are assumed to be proportional to the system size represented by the effective cell-pair area (not covered by the spacer and the gasket). In addition, it is assumed that the operating costs consist only of the energy costs associated with the stack power consumption and the pumping power. As a result of these two assumptions, we can express the total cost of the system as follows:

$$C = K_{\mathrm{m}} A + K_{\mathrm{e}} P \tag{7}$$

where K_{m} is the fixed cost per unit effective cell-pair area per unit time, A is the effective cell-pair area, K_{e} is the cost of electricity, and P is the total power consumption, which is the sum of stack power consumption and pumping power. The minimization of the total cost is a trade-off between the fixed costs and the operating costs. Equation 7 can be divided by the cost of electricity, K_{e} to get a normalized cost:

$$c^* = \frac{C}{K_{\mathrm{e}}} = rA + P \tag{8}$$

where r is the cost ratio:

$$r = \frac{K_{\mathrm{m}}}{K_{\mathrm{e}}} \tag{9}$$

At the cost-optimal system size, A_{opt}, the derivative of the normalized cost is zero:

$$\left(\frac{\partial c^*}{\partial A}\right)_{A=A_{\mathrm{opt}}} = r + \left(\frac{\partial P}{\partial A}\right)_{A=A_{\mathrm{opt}}} = 0 \tag{10}$$

and the derivative of the power consumption is:

$$\left(\frac{\partial P}{\partial A}\right)_{A=A_{\mathrm{opt}}} = -r \tag{11}$$

At each system size, the velocity and channel height are chosen such that the power consumption is minimized. As a result, the power consumption is only a function of the system size, irrespective of the cost factors. At the optimal system size, the increase in cost due to the marginal increase in system size is exactly offset by the decrease in cost due to the marginal decrease in power consumption, which is why the optimal system size is only a function of the cost ratio, r, as shown in Eq. 11, and is not a function of the unit fixed cost or the cost of electricity separately. If both K_{m} and K_{e} are changed such that their ratio is held constant, the optimal system size is not affected. This is beneficial because these costs vary greatly by location, and it is difficult to determine with any certainty what value of K_{m} should be used. In this paper, we focus on the framework that should be used for the optimization of ED systems, and we study the different trade-offs

that need to be understood in the optimization of these systems. The results of this study are general, and can be used for any values of K_m and K_e.

As an example of how the normalization results presented in the following sections should be interpreted, we provide a sample calculation of the cost ratio, r. Table 1 shows typical values of the variables needed to calculate the cost ratio. The interest rate, i, and the plant life, τ, are required to amortize the capital expenses:

$$K_m = \frac{K_{m,0}}{\frac{1}{i}\left[1 - \left(\frac{1}{1+i}\right)^{\tau}\right]} \tag{12}$$

where $K_{m,0}$ is the present value of the equipment costs.

Table 1: The variables used in the cost modeling examples in the following sections [26]. The resulting cost ratio is $r = 134\ \mathrm{W/m^2}$.

Variable	**Value**
Cost of electricity, K_e	\$0.15/kWh
Present value of equipment costs, $K_{m,0}$	$\$1,500/\mathrm{m^2}$ effective cell pair
Rate of return on capital, i	10%
Plant life, τ	20 years

4. Design and operation of a system of fixed size: Effect of channel height and fluid velocity on energy consumption

In this section, we study the effect of the channel height and the fluid velocity on the power consumption of systems of fixed membrane area. It must be noted here that, as a result of our assumption that the fixed costs of the system are proportional to the membrane area (Section 3.2), minimizing the power consumption of a system of fixed size also results in the lowest possible total costs.

Figure 3 shows the effect of channel height and velocity on the energy consumption of a fixed-size high-salinity brine concentration system, where the energy consumption is obtained by dividing the power consumption by the volumetric flow rate of the product.

4.1. Effect of channel height on energy consumption

We focus first on the effect of the channel height. Equation 6 shows that the stack energy consumption increases with the channel height, given that the channel resistances are directly proportional to their height. In addition, Fig. 3 shows that the lowest channel height results in the lowest total energy consumption. Even though going to a smaller channel height results in higher pumping power, the velocity can be decreased

enough to make the increase in pumping power smaller than the decrease in stack power consumption. This is consistent with previous studies in the literature [14, 15]. Whenever the power consumption is reported to be minimized at a value of channel height that is higher than the lowest value possible, it is because the velocity is not treated as an independent variable, and the increase in pumping power is larger than the decrease in stack power consumption [16].

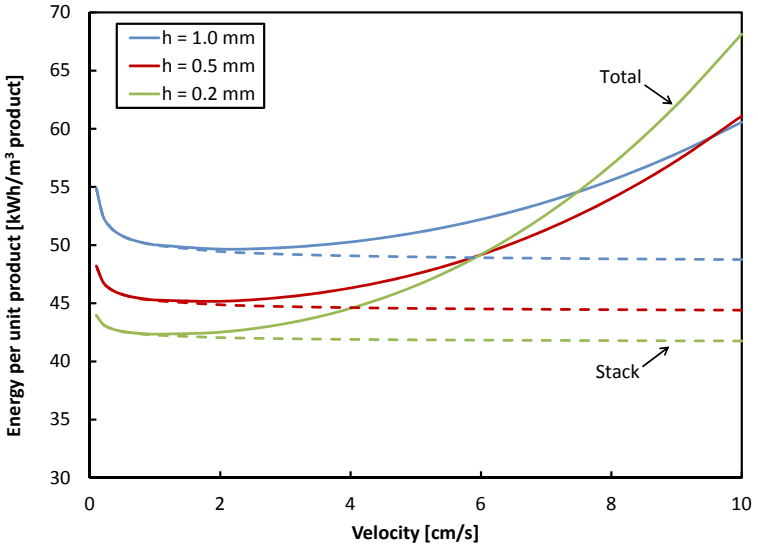

Fig. 3: Effect of channel height and velocity on the energy consumption of a fixed-size ED system for high-salinity brine concentration with $S_{\text{feed}} = 70$ g/kg. The solid line indicates the total energy consumption, the dashed line indicates the stack energy consumption, and the difference between the two lines is the pumping energy consumption. The simulated membrane area is the one that leads to the lowest total cost Section 6.

4.2. Effect of fluid velocity on energy consumption

As shown in Fig. 3, high velocities result in significant pumping requirements, which increases the total energy consumption. This effect pushes the optimal velocity downwards. The total energy consumption decreases with decreasing velocity until low velocities are reached and the stack energy consumption increases significantly.

Fluid velocity affects the stack consumption through its effect on the mass transfer coefficient, or the thickness of the diffusion film, δ, in the stagnant film model, where a higher velocity leads to a thinner diffusion film. As shown in Fig. 4, a larger diffusion film results in stronger concentration polarization, which has two negative effects. The first is that, for the same current density, a thicker diffusion film results in a larger change in concentration between the bulk concentration and the concentration at the interface. This is due to the fact that the slope of the concentration inside the diffusion layer is directly proportional to the current density. The change in concentration at the membrane interface, Δc, that is associated with having a different diffusion layer thickness is shown in Fig. 4. This effect results in a larger trans-membrane

concentration difference, which leads to stronger diffusion and osmosis. With more osmosis and diffusion, more salt needs to be transported to result in the set outlet salinities. This results in a higher total current, which is directly proportional to the amount of salt transported. The second effect is that, in the diluate channel, a thicker diffusion film results in a lower concentration inside the film, which increases the stack resistance. The difference between the two concentration profiles is shown in red in Fig. 4. The increase in stack resistance becomes very significant when the system is operated at close to limiting current density, and the concentration close to the membrane becomes close to zero. This effect is shown in the i-V curves at two different velocities in Fig. 5. The concentrations are set to those at the end of the stack and are not varied. A higher voltage needs to be applied to result in the same current density when the velocity is lower. In the results reported in Fig. 3, a current density of around 400 A/m^2 is required to result in the specified outlet salinity. At that current density, the voltage needs to be around 5% higher for the lower velocity. In addition, the higher velocity allows the system to reach a higher limiting current density, as evidenced by the difference between the two asymptotes.

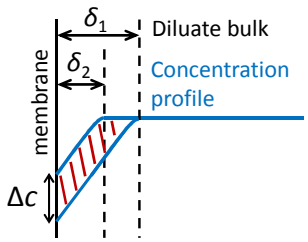

Fig. 4: Schematic diagram showing the effect of the diffusion film thickness, δ, on concentration polarization for two velocities under the same current density.

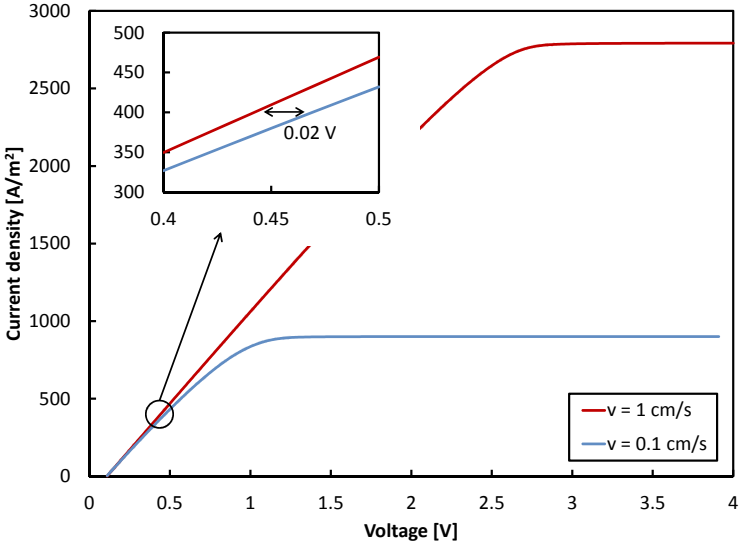

Fig. 5: i-V curves for two different velocities. $h = 0.5$ mm, $S_C = 200$ g/kg, and $S_D = 35$ g/kg.

Table 2 shows the changes in stack power, voltage, current, and resistance that result from going from a

velocity of 1 cm/s to a velocity of 0.1 cm/s, and summarizes the causes for these changes.

Table 2: Effect of decreasing the velocity from 1 cm/s to 0.1 cm/s for the full system with $h = 0.5$ mm, and with the system size that is modeled in Fig. 3.

Variable	**Change**	**Cause of the change**
Stack power consumption, P_{stack}	+6.6%	increase in voltage and current
Voltage, V	+5.2%	increase in current and resistance
Total current, I	+1.3%	increase in diffusion and osmosis
Stack resistance, Ω	+3.9%	lower concentrations inside films

4.3. Optimal channel height and velocity for high-salinity brine concentration and brackish-water desalination

The design and operation of a brackish-water desalination system should follow the same guidelines as those described above for the brine concentration case: as shown in Fig. 6, the channel height should be made as small as possible, and the velocity should be just high enough to decrease the effect of concentration polarization. The velocity should be increased until the increase in the required pumping power becomes equal to the decrease in stack power consumption.

We notice two differences between the two applications. The first is that, for brackish-water desalination, the lowest achievable velocity is dictated by the limiting current density, which explains why the curves do not go below relatively high velocities, and why the thickness of $h = 1$ mm cannot be used for this system size and this velocity range. The second is that the increase in stack power consumption close to the limiting current is not as high as that in the brine concentration case. This is because the total stack resistance is higher in brackish-water desalination and is not strongly influenced by the diffusion film. In addition, the velocity in the brackish application is higher, and the resulting diffusion film is thinner, which means that the increase in film resistance has a smaller effect on the total stack resistance.

5. Minimizing the total cost of ED for brackish-water desalination: Trade-off between ED system size, stack power, and pumping power

The previous section discussed how to design and operate a system of fixed size. In this section, we look at how the system size should be chosen to minimize the total cost of brackish-water ED desalination. This is primarily achieved by finding the average current density that accounts for the trade-off between ED stack capital costs, ED stack power consumption, and pumping power. Increasing the average current density decreases the ED capital costs while increasing ED operating costs. Given that brackish-water ED is constrained by low limiting current densities, the fluid velocity within the stack needs to be increased to

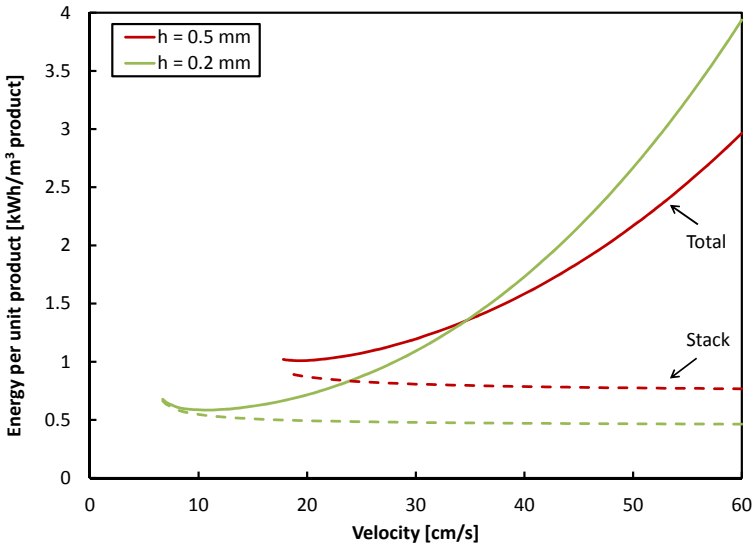

Fig. 6: Effect of channel height and velocity on the energy consumption of a fixed-size ED system for brackish-water desalination with $S_{\text{feed}} = 3$ g/kg. The solid line indicates the total energy consumption, the dashed line indicates the stack energy consumption, and the difference between the two lines is the pumping energy consumption. The simulated membrane area is the one that leads to the lowest total cost in the Section 5.

achieve higher limiting current densities. This results in pumping power playing an important role in the trade-off that determines the optimal system size. The details of this analysis are presented in the paragraphs below.

5.1. Choice of channel height and velocity

Equation 8 shows that, given the minimum power consumption at each membrane area, only the ratio r is required to determine the optimal system size. For each system size, the channel height and the velocity have to be set to result in the lowest power consumption. As mentioned in Section 4, the channel height should be set to the smallest value achievable. This minimum is limited by practical difficulties in designing sealing frames and spacers [15]. For the following results, the channel height is set to 0.5 mm, which is a thickness already used in actual systems [26]. In addition, for each system size, the velocity is set such that the total power consumption is minimized.

5.2. Effect of the average current density on system costs

Figure 7 shows the variation of the normalized cost of water production with the average current density. Average current density can be thought of as a measure of the inverse of the system size. As the system size decreases, the same amount of salt needs to be removed through a smaller area, which results in a higher average current density. This explains why fixed costs decrease as the average current density increases. As predicted by Eq. 6, the stack power consumption increases with the average current density. The fixed costs of the system dominate at low current density, which pushes the system operation to higher current densities.

Due to the low concentration in the diluate channel, the limiting current density is low, and the velocity needs to be increased to increase the limiting current density, as shown in Fig. 5. The increased limiting current density comes with the cost of a higher pumping power, which determines how much the operating current can be increased before the increase in energy costs starts outweighing the decrease in fixed costs. It is this trade-off between fixed costs and energy costs (both stack and pumping energy) that determines the optimal operating current density and system size.

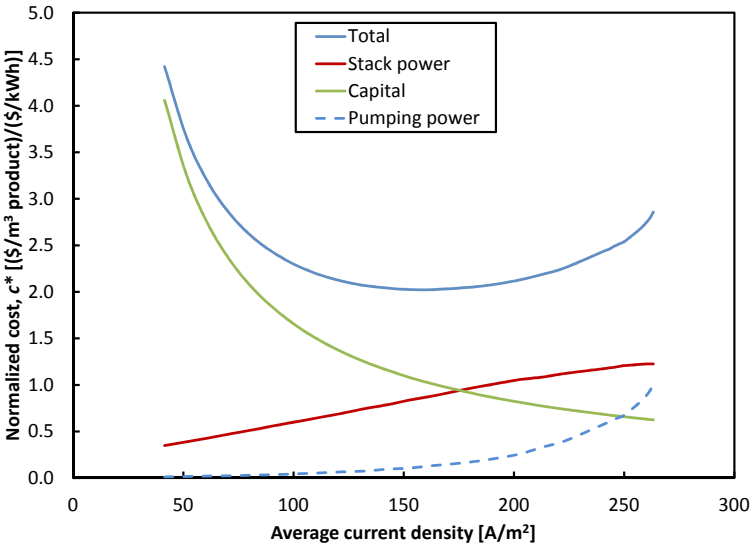

Fig. 7: Normalized cost of a brackish-water desalination system which desalinates a feed from 3 g/kg at 80% recovery and produces 1 m^3/s of product at 0.35 g/kg. $r = 134$ W/m^2.

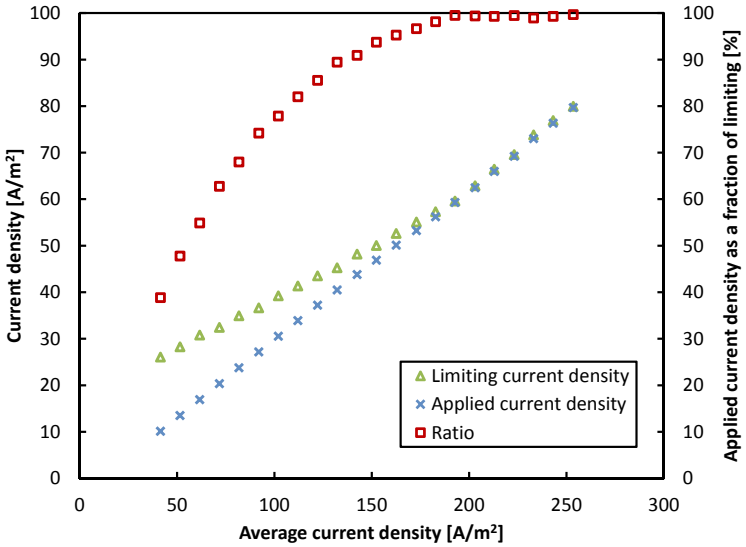

Fig. 8: Ratio of operating current to limiting current for brackish-water desalination.

Figure 8 shows the variation of the applied current density and the limiting current density at the outlet of the ED stack, as well as their ratio, with the average current density. As expected, the applied current

density at the outlet of the system varies linearly with the average current density. The current density at the outlet is much smaller than the average given that it is the smallest current density anywhere in the stack because it occurs at the point with the lowest diluate concentration. The limiting current density must increase with the average current density in order to allow the higher current densities to be reached. We note that applied current density is only equal to the limiting current density for systems with an average current density higher than around 200 A/m^2. For systems with a smaller average current density, more pumping power is spent than is necessary to achieve a limiting current density equal to the applied current density. This is the case because the velocity in those cases is small, and the excess pumping power is smaller than the savings in stack power consumption due to operating away from the limiting current regime, as explained in Section 4. As the applied current density increases, the velocity needs to be increased to result in a limiting current density that is at least equal to the applied current density. At these high velocities, the savings in ED stack consumption no longer justify the excess pumping power, and the velocity is just high enough to allow the operation under the applied current. As explained in Section 4, this trade-off between pumping power and stack power consumption determines how far from the limiting current density the system should be operated. For a cost ratio equal to 134 W/m^2, the applied current density at the outlet of the stack is equal to around 94% of the limiting current density. This number is strongly dependent on the relationship between pumping power and stack power consumption, which is a result of the spacer design and the resulting Sherwood number and friction factor relations.

5.3. Impact of optimization of velocity and system size on system costs

In this section, we highlight the benefit of optimization by looking at the impact that deviations of velocity and system size from their optimal values have on system costs. In Table 3, the increase in cost due to improper operation and sizing is quantified. First, we look at the effect that deviations in velocity have on the final costs of the system. For every system size, the velocity is set to 50% larger than the optimal velocity at that size. The minimum cost is 6% higher than that obtained using the optimal velocity. At a velocity 50% lower than the optimal velocity, the cost increases by 33%, a very significant increase. This is because a low velocity results in a low limiting current density, which limits the average current density and leads to unnecessarily large systems.

Next, we look at the effect that deviations in system size have on the final costs. Using the cost numbers presented in Fig. 7, the cost increases by 9% when a system that is oversized by 50% is used. When a system 40% smaller than the optimal size is used, the cost increases by 38%, a significant increase. The increase in cost is higher when the system size is decreased than when it is increased. This is due to the effect of the limiting current density. Starting at the cost-optimal system size, the system size can only be decreased by

greatly increasing the velocity, which is required to increase the limiting current density. This results in a large increase in pumping power, and greatly increases the total cost. In addition, the decrease in system size is constrained by the limiting current density, and a 50% decrease in system size is not possible in this case without going to very high velocities. In addition, these numbers show the effect of having only one variable being suboptimal, with the other being optimized. We can expect the cost numbers to be even worse when no optimization is performed. This shows the importance of choosing the optimal velocity and system size for the minimization of the cost of brackish-water desalination.

Table 3: Effect of operating away from the optimal velocity and the optimal system size in the brackish-water desalination application. $r = 134$ W/m^2.

Deviation from the optimal	**Resulting increase in cost**
Velocity increase of 50%	+6%
Velocity decrease of 50%	+33%
System size increase of 50%	+9%
System size decrease of 40%	+38%

5.4. Optimal operating conditions at different cost ratios

The results shown above are for a cost ratio equal to 134 W/m^2. Given that the minimum power consumption was calculated for a range of system sizes, the cost ratio can be varied, and the optimal operating points can be determined at each cost ratio. Figure 9(a) shows the variation of the optimal effective cell-pair area and average current density with the cost ratio, r. As expected, as the ratio increases, the relative importance of the fixed costs increases, and the optimal system size becomes smaller. As shown in Fig. 9(b), making the system smaller requires increasing the limiting current density, which results in a higher velocity at higher cost ratios. Equations 4 and 5 can be combined by eliminating $N_{\mathrm{cp}}W$ to result in the following equation:

$$L = \frac{Ahv}{Q_{\mathrm{product}}} \tag{13}$$

Equation 13 shows that the length, L, is proportional to the product of the velocity, v, and the area, A. Figure 9 shows that the decreasing area and the increasing velocity result in an increase in the optimal length with the cost ratio. We note that the membrane areas and the lengths reported are the effective area and length, and that real systems usually only use 65% of the total area effectively for mass transfer [26–28], so we expect the *physical* membrane area of these systems to be approximately 50% larger than the effective values reported above. We also note that the reported cost modeling is not dependent on the fraction of the area used effectively because it uses the effective cell-pair area. By using the effective area in the cost

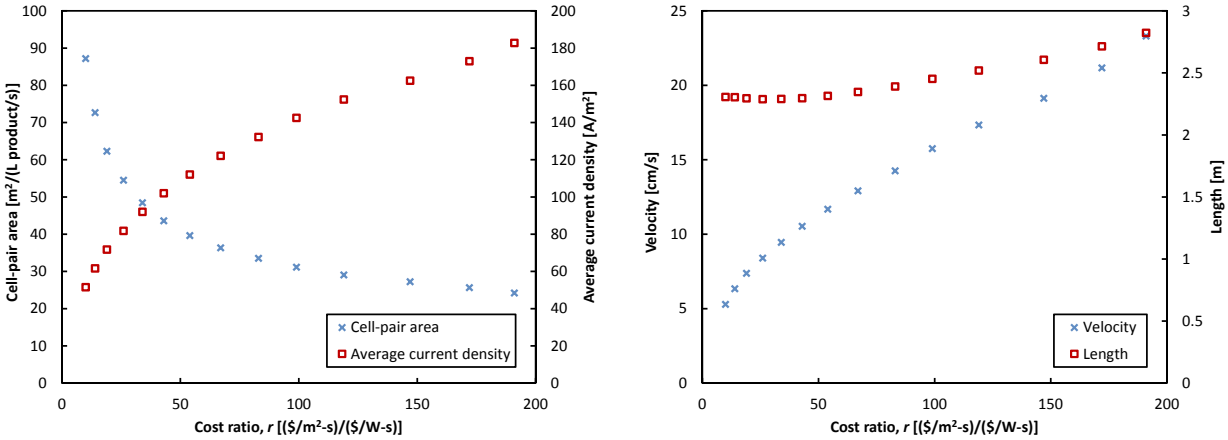

(a) Variation of the optimal effective area and average current density with the cost ratio.

(b) Variation of the optimal velocity and effective stack length with the cost ratio.

Fig. 9: Effect of the cost ratio on the system size and on design and operation variables for brackish-water desalination.

modeling, we ensure that the results presented in this work are not dependent on the fraction of the area used effectively. For a given effective fraction, the total membrane area and the physical stack length can be calculated from the effective values presented above.

Figure 10 shows that the ratio of the applied current density to the limiting current density increases with increasing cost ratio. This can be explained by the increase of the average current density with increasing cost ratio (shown in Fig. 9(a)), and the analysis of the trends reported in Fig. 8. In addition, the optimal limiting-current ratio strongly depends on the cost ratio, and it is *not* sufficient to use a general ratio as is commonly done in the literature.

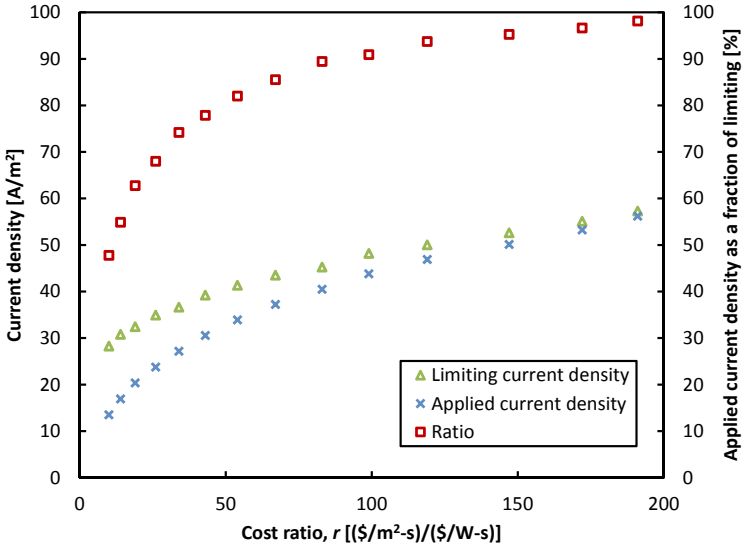

Fig. 10: Variation of the ratio of operating current to limiting current with the cost ratio for brackish-water desalination.

Finally, the normalized cost of water production can be expressed as a function of the cost ratio r. For

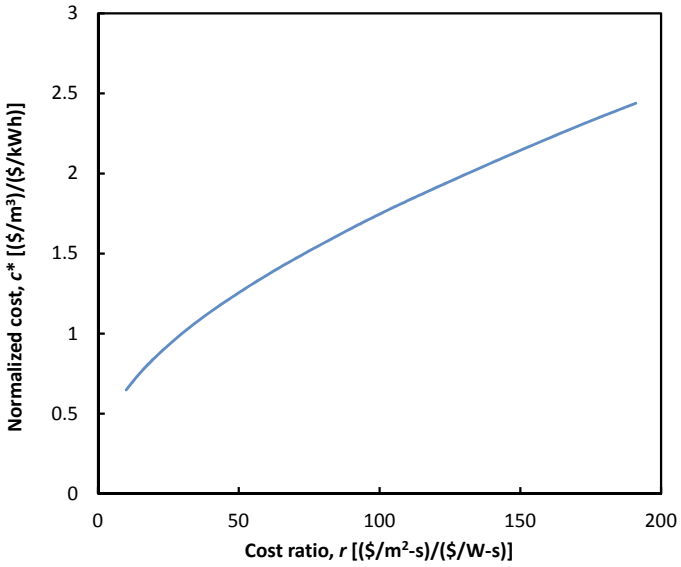

Fig. 11: Variation of the normalized cost with the cost ratio for brackish-water desalination.

any cost ratio (calculated based on local cost numbers), Fig. 11 gives the cost of producing 1 m^3/s of water at 0.35 g/kg and at a recovery of 80% starting with a feed at 3 g/kg. The normalized cost is then easily multiplied by the local cost of electricity expressed in \$/kWh to give the actual cost of water production, which for the cost numbers reported in Table 1 is around \$0.3 per m^3 of product.

6. Minimizing the total cost of ED for high-salinity brine concentration: Limited effect of pumping

In this section, we study the cost minimization of ED for high-salinity brine concentration. As in Section 5, the channel height is set to 0.5 mm, and, for every system size, the velocity is chosen such that the power consumption is minimized.

6.1. Effect of average current density on system costs

Figure 12 shows the variation of the costs associated with brine concentration with the average current density, which is inversely proportional to the system size. The fixed costs, which are proportional to the system size, are inversely proportional to the average current density. In addition, the stack power consumption is linearly proportional to the average current density. This is consistent with the fact that the dominant resistance at high salinity is that of the membranes [24], which is assumed constant. Further, the pumping cost is negligible for all system sizes. As shown in Fig. 13, the limiting current density is fairly high because of the high concentrations, and, as a result, high velocities are not needed to increase the limiting current density. The trade-off between fixed costs and stack energy costs is what determines the optimal system size and optimal average current density without any influence from the pumping costs.

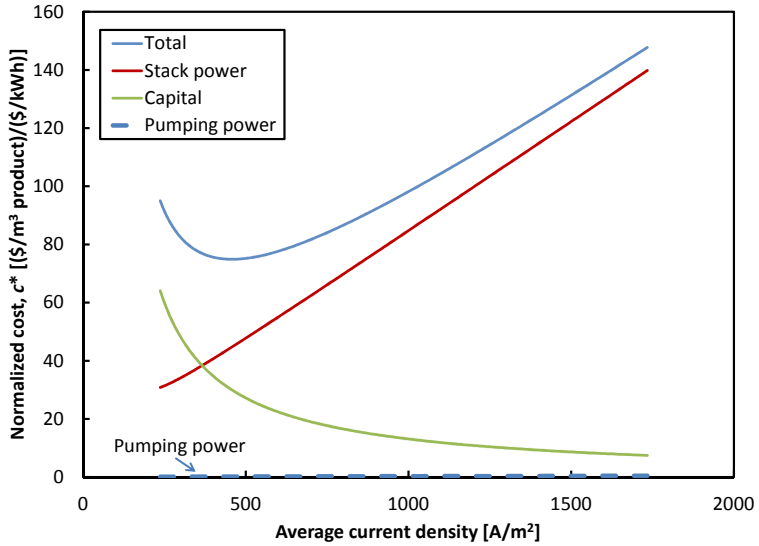

Fig. 12: Normalized cost of a high-salinity desalination system which concentrates a feed of 70 g/kg and produced 1 m^3/s of product at 200 g/kg. $r = 134$ W/m^2.

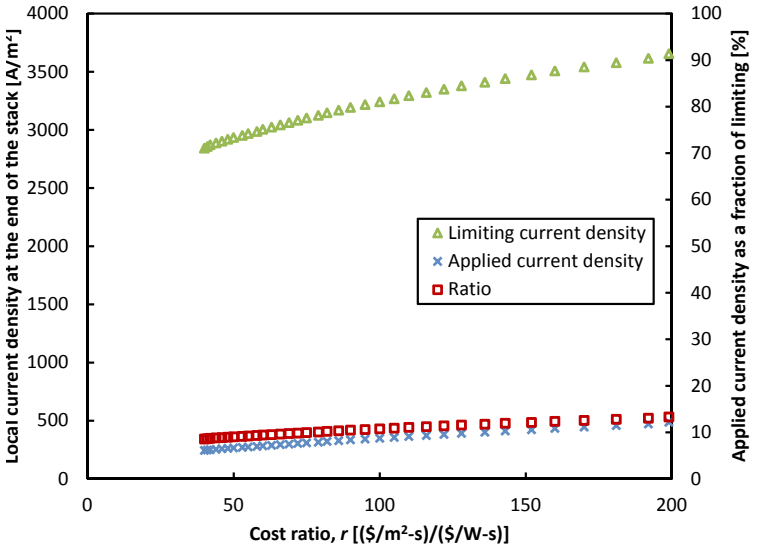

Fig. 13: Variation of the ratio of operating current to limiting current with the cost ratio for high-salinity brine concentration.

6.2. Impact of optimization of velocity and system size on system costs

In this section, we highlight the benefit of optimization by looking at the impact that deviations of velocity and system size from their optimal values have on system costs. In Table 4, the increase in cost due to improper operation and sizing is quantified. It can be seen that, in brine concentration, velocity affects the system cost much less than in brackish-water desalination (Table 3). A 50% deviation in velocity from the optimal value results in only a 2%-3% increase in the system cost. This follows from the fact that, in brine concentration, velocity has a low effect on ED stack power consumption, and, near the optimal velocity, the pumping power is negligible, as shown in Fig. 12. That said, even a 2% increase in total cost may be

significant when designing large plants. System size, however, significantly affects the costs. When a system is undersized by 50%, the cost increases by 22%. Oversizing increases costs to a lesser extent, with a system 50% larger than optimal increasing costs by 7%. These numbers show that it is important to properly size an ED brine-concentration system and to operate it under the optimal average current density, and that undersizing a system (i.e., operating under a higher than optimal current density) has a higher penalty on costs than oversizing.

Table 4: Effect of operating away from the optimal velocity and the optimal system size in the brine-concentration application. $r = 134$ W/m^2.

Deviation from the optimal	**Resulting increase in cost**
Velocity increase of 50%	+2%
Velocity decrease of 50%	+3%
System size increase of 50%	+7%
System size decrease of 50%	+22%

6.3. Optimal operating conditions at different cost ratios

Figure 14(a) shows the variation of the optimal cell-pair area and the average current density with the cost ratio, r. As discussed in Section 5, the higher cost ratio increases the relative importance of fixed costs, and pushes the optimum towards lower areas and higher current densities. The required cell-pair area and average current density are both higher in brine concentration than in brackish-water desalination because of the much higher quantity of salt to be transported in taking a feed from 70 g/kg to 200 g/kg than in taking a feed from 3 g/kg to 0.35 g/kg.

Figure 14(b) shows the variation of the velocity and stack length with the cost ratio. The velocity here is at the outlet of the concentrate, and, given the low system recovery of around 21%, the velocity at the outlet of the diluate channel is around 4 times higher. Given the high water transport in brine concentration, the flow rates change significantly over the length of the system. This variation in velocity should be kept in mind when interpreting these results. The optimal velocity increases with the cost ratio. At higher cost ratios, the average current density is higher, and, as a result, the relative importance of stack power consumption compared to pumping power is higher. This pushes the optimal velocity upwards as explained in Section 4. The stack length decreases with the cost ratio because the decrease in area is more significant than the increase in velocity, as explained by Eq. 13.

Figure 15 shows the normalized cost of producing 1 m^3/s of a saline solution at 200 g/kg at a recovery of 21%, starting with a feed at 70 g/kg. The normalized cost can be multiplied by the local cost of electricity

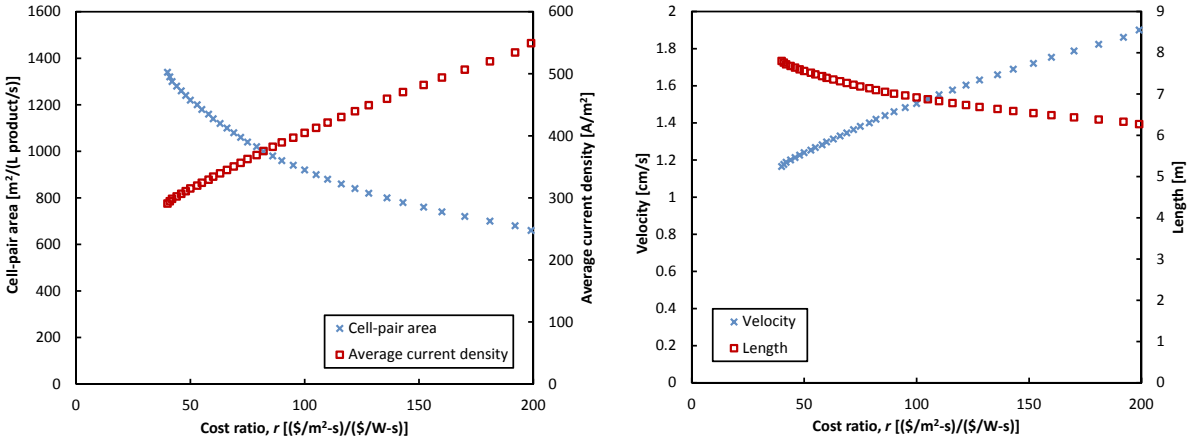

(a) Variation of the optimal effective area and average current density with the cost ratio.

(b) Variation of the optimal velocity and effective stack length with the cost ratio.

Fig. 14: Effect of the cost ratio on the system size and on design and operation variables for high-salinity brine concentration.

to give the total cost. This set of results serves to generalize the analysis, and allows the estimation of the optimal membrane area, average current density, velocity, length, and cost of brine concentration under different cost scenarios. For the cost numbers presented in Table 1, the cost of brine concentration is around \$11 per m^3 of product at 200 g/kg.

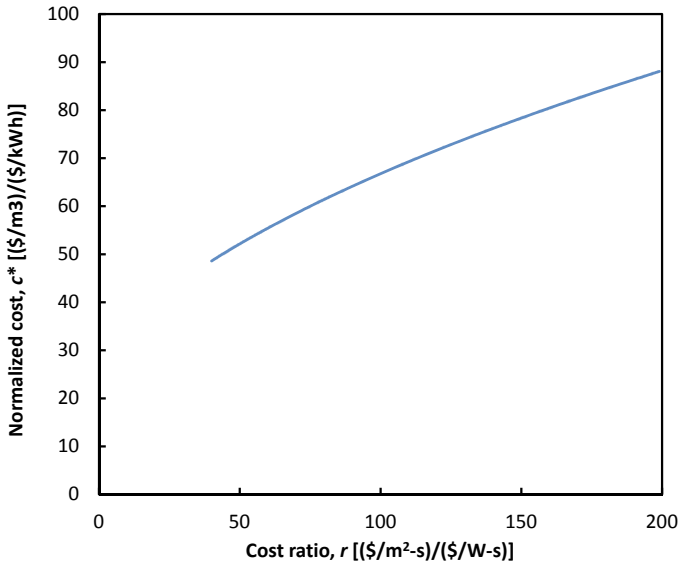

Fig. 15: Variation of the normalized cost with the cost ratio for high-salinity brine concentration.

7. Conclusions

In this paper, a fair set of constraints was developed to thoroughly study the optimal design and operation of ED systems both for brackish-water desalination and for high-salinity brine concentration. The major

conclusions from this work are the following:

1. The channel height should always be minimized. The reduction in the channel height also results in a reduction in stack length, so future improvements that lead to decreasing the channel height will also result in a decrease in the optimal stack length.
2. The optimal velocity is determined by a trade-off between pumping power and ED stack power consumption. It should be small enough to reduce pumping power, but just high enough to increase the limiting current density and to limit concentration polarization.
3. The ratio of the operating current density to the limiting current density in brackish-water desalination is determined by a trade-off between pumping power and ED stack power consumption. This ratio is dependent on the spacer design and on the cost factors.
4. Different trade-offs govern the design of brackish-water desalination and of high-salinity brine concentration:
    - In the desalination of brackish water, the optimal system size is determined by a trade-off between fixed costs on one end, and pumping power and stack power consumption on the other end.
    - In high-salinity brine concentration, the optimal system size is determined by a trade-off between fixed costs and stack power consumption. Pumping costs are negligible because the system operates far from the limiting current regime.

In addition, optimal values of effective cell-pair area, average current density, velocity, effective stack length, ratio of operating current density to limiting current density, and cost have been presented as a function of the cost ratio, r, which includes the effects of the different cost factors that vary greatly with location and possibly with time.

Acknowledgments

The authors would like to thank Kuwait Foundation for the Advancement Sciences (KFAS) for their financial support through Project No. P31475EC01.

Appendix A. Modeling of the diffusion films

The stagnant film model captures the effect of convection without the need to solve the Navier-Stokes equations. The model assumes a perfectly mixed fluid inside the channel, except for a thin diffusion layer near the membranes. The thickness of the diffusion film is calculated from the correlation by Kuroda et al. [22], as detailed in Appendix F. Inside the diffusion film, there are three species (anion, cation, and water),

which results in two independent Maxwell-Stefan (MS) equations. These equations are used to calculate the concentration and electric potential profiles inside the diffusion films. These profiles give the concentration at each membrane interface, and the film potential drops in Eq. 6. The general MS equation can be written as:

$$-c_i \nabla \ln a_i - \frac{z_i c_i F}{RT} \nabla \Phi = \sum_{j=1}^{n} \frac{c_j J_i - c_i J_j}{c_{tot} Đ_{ij}} \tag{A.1}$$

where c_i is the molar concentration of species i, a_i is the activity of species i, $Đ_{ij}$ are the MS diffusion coefficients, J_i the mole flux of species i, and Φ is the electric potential. The left-hand side of Eq. A.1 is the gradient in the electrochemical potential of species i.

In addition, electroneutrality is satisfied inside the diffusion film because the electric double layer is assumed to be a part of the membrane interface:

$$\sum_i z_i c_i = 0 \tag{A.2}$$

The MS model has a major advantage in describing the transport inside the diffusion films. This model allows the integration of the concentration profile, which is important to be able to model the curvature of the i-V curves presented in Fig. 5. Simply calculating the change in concentration between the bulk and the membrane is enough to estimate the limiting current density, but it does not account for the gradual increase in the film resistance as the operating current density gets closer to the limiting current density.

In addition, we note that the concentration in the diluate channel reaches zero close to the CEM. This is because the diffusion coefficient of Na^+ is lower than that of Cl^-, as shown in Table D.5. Given the assumption of the same diffusion layer thickness on both sides of the channel, the effect of concentration polarization is stronger near the CEM.

Appendix B. Modeling of the transport through the membranes

Appendix B.1. Brackish-water desalination

The concentration in the solution just outside the membrane is calculated as described in Appendix A. At the interface, each species that exists in solution and inside the membrane is assumed to be in equilibrium:

$$\mu_i^{\mathrm{m}} = \mu_i^{\mathrm{s}} \tag{B.1}$$

$$RT \ln a_i^m + z_i F \phi^m = RT \ln a_i^s + z_i F \phi^s \tag{B.2}$$

where μ_i^{m} is the electrochemical potential inside the membrane, and μ_i^{s} is that inside the solution. Equation B.2 can be rearranged to get the following expression for the Donnan potential:

$$\Delta\phi_{\mathrm{Donnan}} = \phi^m - \phi^s = \frac{RT}{z_i F} \ln \frac{a_i^s}{a_i^m} \tag{B.3}$$

Equation B.3 can be written for the cation and the anion, and the two expressions can be equated to result in the following equation

$$\frac{c_+^s c_-^s}{c_+^m c_-^m} = \frac{\gamma_\pm^{m\,2}}{\gamma_\pm^{s\,2}} \tag{B.4}$$

where the activity coefficient of the salt inside the membrane, $\gamma_\pm^m$, can be determined experimentally [23]. This equation can be combined with the electroneutrality equation inside the membrane, which is the same as Eq. A.2 but including the membrane fixed charge. Combining the electroneutrality equation with Eq. B.4 allows the calculation of the concentrations of the co-ion and counter-ion inside the membrane. Once the ionic concentrations inside the membrane are known, Eq. B.3 can be used to calculate the Donnan potential at each interface. The two expressions of Eq. B.3 can be averaged to cancel out the activity coefficient of the separate ions by assuming that $\gamma_+ = \gamma_-$:

$$\Delta\phi_{\mathrm{Donnan}} = \frac{\Delta\phi_{\mathrm{Donnan,+}} + \Delta\phi_{\mathrm{Donnan,\text{-}}}}{2} \approx 0.5 \frac{RT}{F} \ln \frac{c_-^m}{c_+^m} \tag{B.5}$$

The water concentration inside the membrane and the membrane charge are calculated based on empirical measurements made by Kraaijeveld et al. [23]. These are the concentrations used for the calculation of the salt and water fluxes through the membranes. The MS equations inside the membranes are used to calculate the resistive membrane electric potential drop, which is added to the Donnan potential to form the complete potential drop across the membrane used in Eq. 6. The MS equations are also used to calculate the ionic and water fluxes. There are four species inside the membrane (counter-ion, co-ion, water, and membrane fixed charge), which results in three independent MS equations for each membrane. In addition, the diffusion coefficients inside the membrane are different than those in the free solution. The details of this model are available in previous studies [23, 24, 29]. Our numerical implementation of this model was validated with experimental results from Kraaijeveld et al. [23, 29]. The validation was presented in a previous work [24], and is shown again in Fig. B.16. The membrane characteristics used in this model are presented in Appendix D.

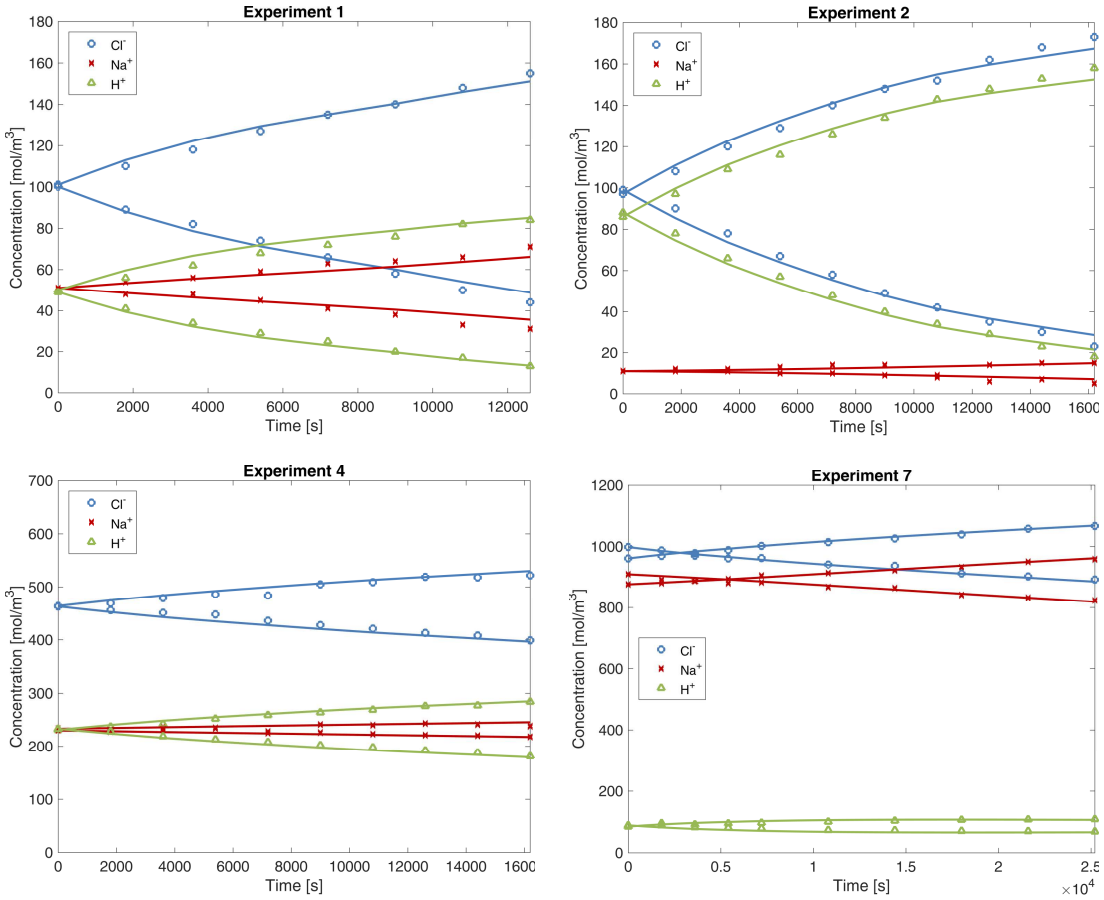

Fig. B.16: Validation of the model using experiments from the literature [29]. The symbols represent experimental values and the solid lines represent the modeling results. This validation has been presented in a previous work [24].

Appendix B.2. High-salinity brine concentration

The Nernst-Planck-based model developed by Fidaleo and Moresi [25] is used to calculate the salt and water fluxes through the membranes in the concentration of high-salinity brines. The salt flux in this model is assumed to be a result of electro-migration and diffusion:

$$J_{\mathrm{s}} = \frac{T_{\mathrm{s}} i}{F} - L_{\mathrm{s}} \left(c_{\mathrm{s,C,m}} - c_{\mathrm{s,D,m}} \right) \tag{B.6}$$

and the water flux is a result of electro-osmosis and osmosis:

$$J_{\mathrm{w}} = \frac{T_{\mathrm{w}} i}{F} + L_{\mathrm{w}} \left(\pi_{\mathrm{C,m}} - \pi_{\mathrm{D,m}} \right) \tag{B.7}$$

where the subscript 's' denotes the salt, the subscript 'w' denotes the water, J is the molar flux, i is the current density, $c_{\mathrm{s,C,m}}$ is the salt concentration at the membrane interface in the concentrate channel, $\pi_{\mathrm{D,m}}$ is the osmotic pressure at the membrane interface in the diluate channel, T_{s} is the salt transport number,

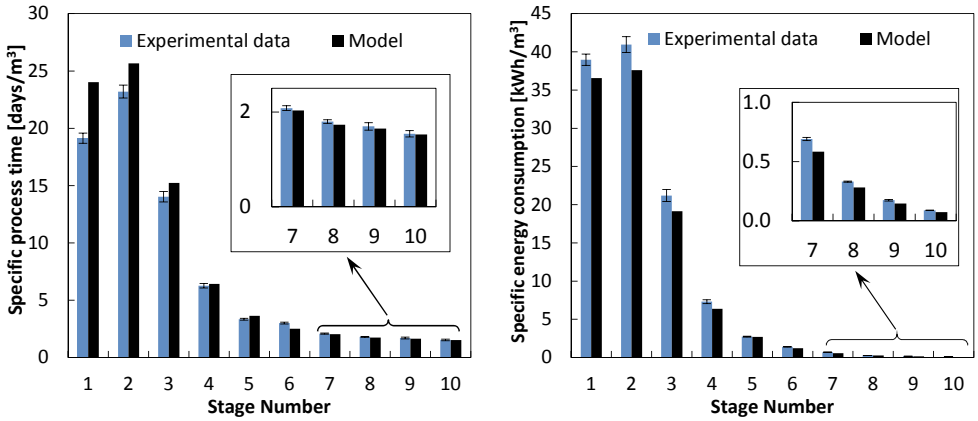

(a) Specific process time, which is a measure of system size defined and reported by McGovern et al. [26].

(b) Specific energy consumption.

Fig. B.17: Validation of the high-salinity model using experimental data from McGovern et al. [26]. Each stage is a batch system which takes the diluate from a given salinity to another set salinity.

and L is the permeability. The transport numbers and permeabilities of salt and water used in this paper were measured at high salinity by McGovern et al. [26].

The fluxes inside the membranes are the same as those inside the adjacent diffusion films. The use of the MS equations inside the diffusion films involves the fluxes of each of the different species, whereas the model used to predict the transport through the membranes only uses the cell-pair salt and water fluxes. In matching the two sets of fluxes, the AEM and CEM are assumed to have the same transport and permeability numbers: the salt flux is the same in the two membranes, and the amount of current density carried by the counter-ion is the same in the two membranes. This allows the matching of the fluxes inside the diffusion films and those inside the membranes.

Finally, the potential drop across the membranes is calculated as the sum of the membrane ohmic potential drops and the Donnan potential:

$$\Delta\Phi_{\mathrm{CEM}} + \Delta\Phi_{\mathrm{AEM}} = (r_{\mathrm{CEM}} + r_{\mathrm{AEM}})\, i + \frac{\Delta\mu_{\mathrm{s}}}{F} = (r_{\mathrm{CEM}} + r_{\mathrm{AEM}})\, i + 2\frac{RT}{F} \ln \frac{\gamma_{\pm,\mathrm{C}} m_{\mathrm{C,m}}}{\gamma_{\pm,\mathrm{D}} m_{\mathrm{D,m}}} \tag{B.8}$$

where $\gamma_{\pm}$ is the mean molal activity coefficient, and m is the molality. The resistances of the membranes, r_{CEM} and r_{AEM}, were measured experimentally by McGovern et al. [26]. The membrane characteristics used in this model are presented in Appendix D. The validation of this model with experimental data from McGovern et al. [26] is shown in Fig. B.17.

Appendix C. Solution method

The models presented in Appendix A and Appendix B allow the calculation of the fluxes of the species and the current density at a given location along the stack. These fluxes are used to update the concentrations and flow rates along the stack. The length of the stack is discretized into sufficiently small elements, and the finite-difference method is used to perform a species balance on each channel. We provide the example of the conservation of salt in the diluate channel:

$$N_{\mathrm{s},i+1} = N_{\mathrm{s},i} - J_{\mathrm{s}}\, dA \tag{C.1}$$

where $N_{\mathrm{s},i}$ is the molar rate of salt in mol/s in element i, $J_{\mathrm{s},i}$ is the salt flux through the cell pair (two membranes), and dA is the finite area associated with the element.

Given the inlet and outlet salinities and flow rates, and given the dimensions of a stack (A, L, W, h), and the velocity at the product outlet, the required applied voltage needs to be determined.

In the brackish-water desalination case, the feed flow rate is given, but its division between the concentrate and the diluate channel needs to be such that the product flow rate is equal to 1 m^3/s. By contrast, the flow rates at the outlet of the stack can both be known by forcing the condition that the concentrate outlet volumetric flow rate be equal to that of the product. This is consistent with having the same channel height and velocity in the two channels. Given the flow rates and salinities at the outlet of stack, and by guessing a value of the applied voltage, the concentrations and flow rates in the two channels can be calculated using a species balance until the inlet of the stack is reached. At the inlet, the calculated diluate concentration is compared to the set inlet concentration, and the voltage guess is updated using the bisection method until convergence is reached. The allowed uncertainty on this value is set to 0.1% to ensure smooth curves. This ensures that numerical errors are negligible when comparing different velocities and system sizes. The node where mixing occurs before the concentrate inlet is used to check that the species are conserved and that there are no errors in the procedure.

In the high-salinity brine concentration case, a similar approach is followed. The outlet flow rates and salinities are known. The voltage is guessed and the concentrations and flow rates in the two channels are calculated until the inlet is reached. At the inlet, the diluate and concentrate concentrations must be equal to the feed concentration. This condition is used to update the applied voltage using the bisection method until convergence is reached.

Table D.5: The diffusion coefficients in the diffusion films [23]. Original data from Chapman [30] and Mills and Lobo [31]. c is the solution concentration in mol/m^3.

Components	**Diffusivity** [10^{-9} m^2/s]
Na^+, H_2O	1.333
Cl^-, H_2O	2.033
Na^+, Cl^-	0.0015 $c^{0.65}$

Table D.6: The diffusion coefficients inside the membranes (in 10^{-10} m^2/s), measured and calculated by Kraaijeveld et al. [23].

Components	**61 CZL 386**	**204 UZL 386**
Na^+, Cl^-	0.24	0.19
Na^+, H_2O	3.12	0.75
Na^+, Membrane	0.31	0.16
Cl^-, H_2O	1.81	5.12
Cl^-, Membrane	0.31	0.51
H_2O, Membrane	2.49	4.93

Appendix D. System characteristics

Appendix D.1. Characteristics of the membranes used for brackish-water desalination.

The water concentration inside the membrane is calculated as follows:

$$c_{\mathrm{w}}^{\mathrm{m}} = \frac{\%\mathrm{H_2O} \times \rho_{\mathrm{m}}}{100 M_{\mathrm{w}}} \tag{D.1}$$

where $\%H_2O$ is the membrane water content.

Appendix D.2. Characteristics of the membranes used for high-salinity brine concentration.

The membrane characteristics measured by McGovern et al. [26] and used in this work are for the Neosepta AMX-SB and CMX-SB membranes, and are listed below:

$$r_{\mathrm{CEM}} = r_{\mathrm{AEM}} = 3.5 \times 10^{-4}\ \Omega\ \mathrm{m}^2 \tag{D.2}$$

$$T_{\mathrm{s}} = -4 \times 10^{-6} S_{\mathrm{D}}^2 + 4 \times 10^{-5} S_{\mathrm{D}} + 0.96 \tag{D.3}$$

$$T_{\mathrm{w}} = -4 \times 10^{-5} S_{\mathrm{C}}^2 - 1.9 \times 10^{-5} S_{\mathrm{C}} + 11.2 \tag{D.4}$$

Table D.7: Membrane characteristics measured by Kraaijeveld et al. [23]. c is the solution concentration in mol/L.

Membrane property	**61 CZL 386**	**204 UZL 386**
Capacity [mol/m^3 wet membrane]	1690	1827
Thickness [mm]	0.563	0.551
Density of wet membrane, ρ_{m} [kg/m^3]	1167.5 - 7.5c + 7.5c^2	1100.0 + 15.0c
Salt activity coefficient, $\gamma_{\pm}^{m}$ [-]	0.57 + 0.28c	0.56 + 0.29c
Water content [%]	30.17 - 0.83c	33.38 - 1.42c

$$L_{\mathrm{s}} = 2 \times 10^{-12} S_{\mathrm{D}}^2 - 3 \times 10^{-10} S_{\mathrm{D}} + 6 \times 10^{-8} [\mathrm{m/s}] \tag{D.5}$$

$$L_{\mathrm{w}} = 5 \times 10^{-4} S_{\mathrm{C}}^{-0.416} [\mathrm{mol/m^2\text{-}s\text{-}bar}] \tag{D.6}$$

Appendix E. Thermophysical properties

We model a solution of sodium chloride because of the availability of experimental data on membrane properties in the literature [23, 26]. In addition, sodium chloride is the major component in seawater, and recent studies show close agreement between the properties of the two solutions [32, 33]. The properties of sodium chloride were implemented in MATLAB by Thiel et al. [34, 35] using Pitzer's equations [36–41]. The properties used in our calculations are the solution density, the mean molal activity coefficient, the water activity, and the osmotic pressure.

Appendix F. Spacer properties

The Sherwood number, Sh, and the friction factor, f, were obtained from Kuroda et al. [22]:

$$\mathrm{Sh} = \frac{k_{\mathrm{m}} D_{\mathrm{e}}}{D} = 0.25\ \mathrm{Re}^{\frac{1}{2}} \mathrm{Sc}^{\frac{1}{3}} \tag{F.1}$$

where k_{m} is the mass transfer coefficient, D_{e} is the effective diameter, D is the diffusivity, Re is the Reynolds number, and Sc is the Schmidt number. This correlation is based on the effective diameter, D_{e}, and the thickness of the diffusion film is calculated from the following relation

$$\delta = \frac{D_{\mathrm{e}}}{\mathrm{Sh}} \tag{F.2}$$

The effective diameter is defined as

$$D_{\mathrm{e}} = \frac{2hW\,(1-\epsilon_{\mathrm{s}})}{h+W} \tag{F.3}$$

where h is the channel height, W is the channel width, ϵ_s is the volume fraction inside the channel. Given that $W \gg h$

$$D_e = 2h\,(1-\epsilon_s) \tag{F.4}$$

and

$$\mathrm{Re} = \frac{\rho v D_e}{\mu\,(1-\epsilon_s)} = \frac{2\rho v h}{\mu} \tag{F.5}$$

The Schmidt number is defined as

$$\mathrm{Sc} = \frac{\mu}{\rho D} \tag{F.6}$$

where μ is the dynamic viscosity, ρ is the density, and D is the diffusion coefficient.

The pressure drop inside the ED channel is

$$\Delta P = 4f\frac{L}{D_e}\frac{\rho v^2}{2} \tag{F.7}$$

The friction factor is calculated using the correlation by Kuroda et al. [22]:

$$f = k_f \mathrm{Re}^{-\frac{1}{2}} \tag{F.8}$$

In this paper, we use the properties of spacer A where $k_f = 9.6$ and $\epsilon_s = 0.2$.

In addition, the entrance pressure drop is calculated using correlations developed by Sadri and Floryan [42], but is negligible compared to the friction losses over the length of the stack because $L \gg h$.

References

[1] H. Strathmann, Electrodialysis, a mature technology with a multitude of new applications, Desalination 264 (2010) 268–288. doi:10.1016/j.desal.2010.04.069.
URL http://dx.doi.org/10.1016/j.desal.2010.04.069

[2] H. J. Lee, F. Sarfert, H. Strathmann, S. H. Moon, Designing of an electrodialysis desalination plant, Desalination 142 (2002) 267–286. doi:10.1016/S0011-9164(02)00208-4.
URL http://dx.doi.org/10.1016/S0011-9164(02)00208-4

[3] N. C. Wright, A. G. Winter V, Justification for community-scale photovoltaic-powered electrodialysis desalination systems for inland rural villages in India, Desalination 352 (2014) 82–91. doi:10.1016/j.desal.2014.07.035.
URL http://dx.doi.org/10.1016/j.desal.2014.07.035

[4] W. E. Katz, The electrodialysis reversal (EDR) process, Desalination 28 (1) (1979) 31–40. doi:10.1016/S0011-9164(00)88124-2.

[5] A. E. R. Reahl, Half A Century of Desalination With Electrodialysis, Tech. rep., General Electric Company (2006).

[6] J. Ortiz, E. Expósito, F. Gallud, V. García-García, V. Montiel, A. Aldaz, Desalination of underground brackish waters using an electrodialysis system powered directly by photovoltaic energy, Solar Energy Materials and Solar Cells 92 (12) (2008) 1677–1688. doi:10.1016/j.solmat.2008.07.020.
URL http://linkinghub.elsevier.com/retrieve/pii/S0927024808002535

[7] P. Tsiakis, L. G. Papageorgiou, Optimal design of an electrodialysis brackish water desalination plant, Desalination 173 (2005) 173–186. doi:10.1016/j.desal.2004.08.031.

[8] R. K. McGovern, S. M. Zubair, J. H. Lienhard V, The benefits of hybridising electrodialysis with reverse osmosis, Journal of Membrane Science 469 (2014) 326–335. doi:10.1016/j.memsci.2014.06.040.
URL http://dx.doi.org/10.1016/j.memsci.2014.06.040

[9] R. K. McGovern, S. M. Zubair, J. H. Lienhard V, The cost effectiveness of electrodialysis for diverse salinity applications, Desalination 348 (2014) 57–65. doi:10.1016/j.desal.2014.06.010.
URL http://dx.doi.org/10.1016/j.desal.2014.06.010

[10] M. Turek, Dual-purpose desalination-salt production electrodialysis, Desalination 153 (2002) 377–381. doi:10.1016/S0011-9164(02)01131-1.

[11] Y. Kobuchi, Y. Terada, Y. Tani, The First Salt Plant in the Middle East Using Electrodialysis and Ion Exchange Membranes, Sixth International Symposium on Salt ll (1983) 541–555.

[12] T. Nishiwaki, Concentration of electrolytes prior to evaporation with an electromembrane process, in: R. E. Lacey, S. Loeb (Eds.), Industrial Processing with Membranes, Wiley & Sons, 1972.

[13] Y. Zhang, K. Ghyselbrecht, B. Meesschaert, L. Pinoy, B. Van der Bruggen, Electrodialysis on RO concentrate to improve water recovery in wastewater reclamation, Journal of Membrane Science 378 (2011) 101–110. doi:10.1016/j.memsci.2010.10.036.
URL http://dx.doi.org/10.1016/j.memsci.2010.10.036

[14] A. A. Sonin, M. S. Isaacson, Optimization of flow design in forced flow electrochemical systems, with special application to electrodialysis, Industrial & Engineering Chemistry Process Design and Development 13 (1974) 241–248. doi:10.1021/i260051a009.
URL http://dx.doi.org/10.1021/i260051a009

[15] K. Hattenbach, K. Kneifel, The effect of cell thickness and flow velocity on water cost in desalination by electrodialysis, Desalination 58 (1986) 33–41. doi:10.1016/0011-9164(86)85010-X.
URL http://dx.doi.org/10.1016/0011-9164(86)85010-X

[16] V. Nikonenko, A. Istoshin, M. K. Urtenov, V. Zabolotsky, C. Larchet, J. Benzaria, Analysis of electrodialysis water desalination costs by convective-diffusion model, Desalination 126 (1999) 207–211. doi:10.1016/S0011-9164(99)00176-9.
URL http://dx.doi.org/10.1016/S0011-9164(99)00176-9

[17] M. Turek, Cost effective electrodialytic seawater desalination, Desalination 153 (2003) 371–376. doi:10.1016/S0011-9164(02)01130-X.

[18] E.-Y. Choi, J.-H. Choi, S.-H. Moon, An electrodialysis model for determination of the optimal current density, Desalination 153 (2003) 399–404. doi:10.1016/S0011-9164(02)01134-7.
URL http://dx.doi.org/10.1016/S0011-9164(02)01134-7

[19] R. A. Robinson, R. H. Stokes, Electrolyte solutions, Courier Corporation, 2002.

[20] T. Shedlovsky, The electrolytic conductivity of some uni-univalent electrolytes in water at 25 C, Journal of the American Chemical Society 54 (1932) 1411–1428. doi:10.1021/ja01343a020.
URL http://dx.doi.org/10.1021/ja01343a020

[21] J. F. Chambers, J. M. Stokes, R. H. Stokes, Conductances of concentrated aqueous sodium and potassium chloride solutions at 25 C, The Journal of Physical Chemistry 60 (1956) 985–986. doi:10.1021/j150541a040.
URL http://dx.doi.org/10.1021/j150541a040

[22] O. Kuroda, S. Takahashi, M. Nomura, Characteristics of flow and mass transfer rate in an electrodialyzer compartment including spacer, Desalination 46 (1983) 225–232. doi:10.1016/0011-9164(83)87159-8.
URL http://dx.doi.org/10.1016/0011-9164(83)87159-8

[23] G. Kraaijeveld, V. Sumberova, S. Kuindersma, H. Wesselingh, Modelling electrodialysis using the Maxwell-Stefan description, The Chemical Engineering Journal and the Biochemical Engineering Journal 57 (1995) 163–176. doi:10.1016/0923-0467(94)02940-7.
URL http://dx.doi.org/10.1016/0923-0467(94)02940-7

[24] K. M. Chehayeb, J. H. Lienhard V, Entropy generation analysis of electrodialysis, Desalination 413 (2017) 184–198. doi:10.1016/j.desal.2017.03.001.
URL http://dx.doi.org/10.1016/j.desal.2017.03.001

[25] M. Fidaleo, M. Moresi, Optimal strategy to model the electrodialytic recovery of a strong electrolyte, Journal of Membrane Science 260 (2005) 90–111. doi:10.1016/j.memsci.2005.01.048.
URL http://dx.doi.org/10.1016/j.memsci.2005.01.048

[26] R. K. McGovern, A. M. Weiner, L. Sun, C. G. Chambers, S. M. Zubair, J. H. Lienhard V, On the cost of electrodialysis for the desalination of high salinity feeds, Applied Energy 136 (2014) 649–661. doi:10.1016/j.apenergy.2014.09.050.
URL http://dx.doi.org/10.1016/j.apenergy.2014.09.050

[27] Saltworks, Electrochem Advanced EDR, Brochure.
URL http://www.saltworkstech.com/wp-content/uploads/2015/03/Saltworks_ElectroChem_Product_Sheet_EN.pdf

[28] Asahi Glass Company, SELEMION, Brochure.
URL http://www.selemion.com/SELC.pdf

[29] G. Kraaijeveld, The Maxwell-Stefan description of mass transfer in ion exchange and electrodialysis, Ph.D. thesis, University of Groningen (1994).

[30] T. W. Chapman, Transport properties of concentrated electrolytic solutions, Ph.D. thesis, University of California, Berkeley (1967).

[31] R. Mills, V. M. Lobo, Self-diffusion in electrolyte solutions, Elsevier Science, 1989.

[32] K. G. Nayar, M. H. Sharqawy, L. D. Banchik, J. H. Lienhard V, Thermophysical properties of seawater: A review and new correlations that include pressure dependence, Desalination 390 (2016) 1 – 24. doi:10.1016/j.desal.2016.02.024.
URL http://dx.doi.org/10.1016/j.desal.2016.02.024

[33] K. G. Nayar, G. P. Thiel, M. H. Sharqawy, J. H. Lienhard V, Seawater flow exergy calculations and the minimum energy for seawater desalination: An update, Desalination (Manuscript in preparation).

[34] G. P. Thiel, E. W. Tow, L. D. Banchik, H. W. Chung, J. H. Lienhard V, Energy consumption in desalinating produced water from shale oil and gas extraction, Desalination 366 (2015) 94 – 112. doi:10.1016/j.desal.2014.12.038.
URL http://dx.doi.org/10.1016/j.desal.2014.12.038

[35] G. P. Thiel, J. H. Lienhard V, Treating produced water from hydraulic fracturing: Composition effects on scale formation and desalination system selection, Desalination 346 (2014) 54 – 69. doi:10.1016/j.desal.2014.05.001.
URL http://dx.doi.org/10.1016/j.desal.2014.05.001

[36] K. S. Pitzer, J. J. Kim, Thermodynamics of electrolytes. IV. Activity and osmotic coefficients for mixed electrolytes, Journal of the American Chemical Society 96 (1974) 5701–5707. doi:10.1021/ja00825a004.
URL http://dx.doi.org/10.1021/ja00825a004

[37] K. S. Pitzer, A thermodynamic model for aqueous solutions of liquid-like density, Reviews in Mineralogy and Geochemistry 17 (1987) 97–142.

[38] C. E. Harvie, J. H. Weare, The prediction of mineral solubilities in natural waters: the Na-K-Mg-Ca-Cl-SO_4-H_2O system from zero to high concentration at 25 C, Geochimica et Cosmochimica Acta 44 (1980) 981 – 997. doi:10.1016/0016-7037(80)90287-2.
URL http://dx.doi.org/10.1016/0016-7037(80)90287-2

[39] C. E. Harvie, N. Møller, J. H. Weare, The prediction of mineral solubilities in natural waters: The Na-K-Mg-Ca-H-Cl-SO_4-OH-HCO_3-CO_3-CO_2-H_2O system to high ionic strengths at 25 C, Geochimica et Cosmochimica Acta 48 (1984) 723–751. doi:10.1016/0016-7037(84)90098-X.
URL http://dx.doi.org/10.1016/0016-7037(84)90098-X

[40] K. S. Pitzer, Thermodynamics of electrolytes. I. Theoretical basis and general equations, The Journal of Physical Chemistry 77 (1973) 268–277. doi:10.1021/j100621a026.
URL http://dx.doi.org/10.1021/j100621a026

[41] K. S. Pitzer, J. C. Peiper, R. Busey, Thermodynamic properties of aqueous sodium chloride solutions, Journal of Physical and Chemical Reference Data 13 (1984) 1–102. doi:10.1063/1.555709.
URL http://dx.doi.org/10.1063/1.555709

[42] R. Sadri, J. Floryan, Accurate evaluation of the loss coefficient and the entrance length of the inlet region of a channel, Journal of fluids engineering 124 (2002) 685–693. doi:10.1115/1.1493813.
URL http://dx.doi.org/10.1115/1.1493813

List of Figures